Analysis of comb transducers with sliding teeth

Eugene J. Danicki

Title: Analysis of comb transducers with sliding teeth

Authors: Eugene J. Danicki

PII: S0997-7538(11)00045-3

DOI: 10.1016/j.euromechsol.2011.03.011

Reference: EJMSOL 2697

To appear in: *European Journal of Mechanics / A Solids*

Received Date: 5 November 2010

Revised Date: 6 March 2011

Accepted Date: 25 March 2011

Please cite this article as: Danicki, E.J. Analysis of comb transducers with sliding teeth, European Journal of Mechanics / A Solids (2011), doi: 10.1016/j.euromechsol.2011.03.011

Analysis of comb transducers with sliding teeth

Eugene J. Danicki

Polish Academy of Sciences, IPPT, 5B Pawińskiego Str., Warsaw, 02-106 Poland

Abstract

Ultrasonic comb transducer generates surface acoustic waves on an elastic substrate by periodic traction exerted by its vibrating periodic teeth on the substrate surface. In this paper, the comb teeth are actually sliding elastic spacers between an acoustic buffer and the substrate. The incident wave in acoustic buffer scatters on periodic spacers producing interface waves in the system which transform into Rayleigh waves at the transducer edges. The full-wave theory of interface wave generation is presented, concluded by efficiency estimation of transformation of the incident wave into the surface wave in the substrate and of the surface waves back to bulk waves in the acoustic buffer. Numerical examples presented for all aluminium substrate, buffer and teeth show the 11-teeth comb combined efficiency for generation and detection on the level of -40dB for optimized teeth height.

Keywords: interface waves; Bragg reflection; ultrasonic transducers

1. Introduction

In ultrasonic nondestructive testing of planar structures, surface acoustic Rayleigh or Lamb waves need to be efficiently generated and detected by dedicated ultrasonic transducers. Comb transducers are found advantageous in such applications (Hurley, 1999). Originally (Victorov, 1967), it is a comb with teeth etched in a solid acoustic buffer that delivers bulk longitudinal incident waves to teeth. Applied to the substrate, the vibrating teeth excite surface waves in it.

In fact, an interface wave is generated at the comb-substrate interface which can be quite different from Rayleigh, both in velocity and in the modal shape; it is transformed into Rayleigh wave at the transducer edges only in typical scattering phenomenon; certain part of the the interface power is lost for the scattered bulk waves in the substrate. This loss is smaller if the interface wave differs less in velocity and modal shape from the surface wave propagating on the free substrate surface. The optimal comb should efficiently generate interface waves and provide conditions for their efficient transformation into surface waves.

Typical comb transducer is a quite complicated, asymmetric waveguide for interface waves which, naturally, propagate in both the substrate and the acoustic buffer (in which the comb is etched). The complicated interaction between the comb and the substrate results in both the complicated dispersive relation and the modal shape of interface waves, which generally are difficult for physical interpretation, what should rather be avoided in measurement systems. For this reason, a symmetric system (a modified comb transducer) is proposed and investigated here, where sliding periodic spacers

are applied instead of the etched comb teeth; spacers are in sliding contact with both the substrate and the acoustic buffer.

For presentation clarity, the substrate, the buffer (both being elastic half-spaces $z < -h/2$ and $z > h/2$, respectively, Fig. 1), and also the spacers (of rectangular cross-section of width w and height h) are assumed to be of the same material characterized by the same Lamé constants λ, μ and mass density ρ. The time-harmonic wave-fields are considered with angular frequency ω (the term $\exp(j\omega t)$ will be generally omitted in the presented equations); the corresponding wave-numbers of longitudinal and transversal waves are: $k_l = \omega\sqrt{\rho/(\lambda+2\mu)}, k_t = \omega\sqrt{\rho/\mu}$, respectively, and the Rayleigh wave-number is $k_R > k_t$ (its wavelength is $\lambda_R = 2\pi/k_R$). According to the above discussion, we will seek interface waves with wave-number $k_o \approx k_R$. The analyzed system is infinite in y direction and the plane interface waves propagate along x-axis.

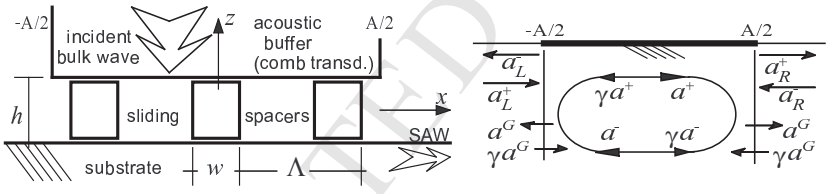

Figure 1: A modified comb transducer with sliding periodic spacers inserted between the acoustic buffer and the substrate. Normal incident longitudinal wave excites interface waves in the system, which transform into Rayleigh waves (SAW) at the comb edges in the scattering/reflection phenomenon, depicted on the right-hand side drawing (to be discussed in Sec. 6; arrows shows the propagation directions of wave-modes).

The paper is organized as follows. Next section presents the model of comb teeth as a h-long piece of free elastic plate of thickness w (Danicki,

2008). A pseudo-acoustic impedance **H** (in the applied notations, boldface letters are reserved for matrices), yields the relation between Fourier components of displacements and stress at both ends of a spacer. The matrix **g** provides analogous characterization of elastic half-spaces sufficient for this analysis: the dependence of normal surface displacements on the normal surface stress. The boundary-value problem for interface waves and the scattering problem for normall incident longitudinal wave-beam on the spacers is considered next, including discussion of numerical examples. Finally, the simplified scattering problem for interface waves at the comb edges is formulated and the comb transducer efficiency is estimated.

In numerical examples presented in Sec. 4 and later, the acoustic buffer and teeth, as well as the substrate are all of aluminium, for which $k_l/k_t = 0.4723$. Taking into account earlier results (Danicki, 1999), we applied narrow teeth of w equal to a quarter Rayleigh wavelength, because narrow teeth makes the interface waves closer to Rayleigh waves, what is favorable for mutual conversion of these waves at the comb edges.

2. Planar wave-fields

The considered harmonic wave-fields $\exp(j\omega t - jpx - jqz)$ are considered to be independent of axis $y = x_2$ in the Cartesian coordinate system $x = x_1, z = x_3$, and satisfying the radiation conditions at $z \to \pm\infty$. The system under consideration consists of three distinct layers: acoustic buffer ($z > h/2$) that supports the incident wave propagating downwards from infinity toward the periodic system of spacers occupying the layer $-h/2 < z < h/2$, and the substrate $z < -h/2$ (Fig. 1). It is convenient for this analysis to

describe these structural components by surface wave-fields at the surfaces of layers, that is at both contact planes of spacers with acoustic buffer and the substrate.

2.1. Wave-field at the substrate surface

Assuming the normal surface traction $T_{33} = t_{33}\exp(j\omega t - jpx)$ at $z = -h/2$ while $T_{31} = 0$, one can easily evaluate the normal surface displacement at this surface as $u_3\exp(j\omega t - jpx)$, where (Danicki, 1999):

$$u_3 = \frac{j}{\mu}\, g t_{33}, \qquad g(p) = \frac{q_t k_t^2}{(2p^2 - k_t^2)^2 + 4p^2 q_l q_t}, \tag{1}$$

and where $q_{l,t} = \sqrt{k_{l,t}^2 - p^2} = -j\sqrt{p^2 - k_{l,t}^2}$ have signs chosen to satisfy the radiation condition at $z =\!\!\rightarrow -\infty$ by the assumed wave-field $\exp(jq_{l,t}z)$ in the substrate.

Substrate loading by surface traction $t_{33} = \mu\zeta u_3$ yields a convenient tool (Ingebrigtsen, 1969) for evaluation of normalized surface displacements. Let $\zeta = z_0 + j\varepsilon$ with $\varepsilon \to 0$ and $\bar{g} = jg(p)$, being a real-valued function for real $p > k_t$. The dispersive equation for the perturbed surface wave is: $\bar{g}^{-1} = \zeta$, with solution $p = k'_R + j\delta$, where $\delta = \varepsilon/\dot{g}$, and:

$$\begin{gathered} \bar{g}^{-1}(k'_K + j\delta) = \bar{g}^{-1}(k'_R) + j\delta\dot{g}, \\ \dot{g} = d\bar{g}^{-1}/dr\ |_{k'_R}; \end{gathered} \tag{2}$$

k'_R can be found numerically from $\bar{g}^{-1}(k'_R) = z_0$; for $z_0 \to 0$, the limit of k'_R is k_R, the wave-number of Rayleigh wave.

The imaginary part of surface wave-number $j\delta$ indicates the wave damping due to the power loss in the surface loading: $P = -\mathrm{Re}\{t_{33}^*(j\omega u_3)\}/2 = -\mu\varepsilon\omega|u_3|^2/2$, which can be compared with the SAW power decaying $\Pi(x) =$

$0.5|a|^2 \exp(-2\delta x)$, where the initial SAW amplitude is defined by $\Pi = |a|^2/2$. This comparison yields:

$$\begin{aligned} \frac{d\Pi}{dx} &= P, \text{ finally:} \\ |a|^2 &= |\frac{\dot{g}}{2}|\mu\omega|u_3|^2, \end{aligned} \tag{3}$$

presenting the dependence of surface displacement u_3 on SAW amplitude for given k'_R. According to Eq. (1), $u_3 \sim t_{33}/(p - k_R)$ indicating that only a surface traction of wave-number close to k_R contributes significantly to the SAW power; the same holds for the corresponding spatial spectra of u_3.

2.2. Wave-field at the buffer surface

In acoustic buffer, the incident wave close to normal and characterized by particle displacement u_3^I and traction t_{33}^I, satisfies the radiation conditions at $z \to \infty$. The scattered wave-field u_3^s, t_{33}^s depends on z differently: $\exp(-jq_{l,t}z)$, what results in different sign of the dependence of u_3^s on t_{33}^s. Explicitly, for a full wave-field at the buffer surface being the superposition of both the incident and scattered fields $u_3 = u_3^s + u_3^I$ on $t_{33} = t_{33}^s + t_{33}^I$, one obtains:

$$\begin{aligned} u_3 - u_3^I &= \frac{-j}{\mu}\, g(t_{33} - t_{33}^I), \\ \text{that is: } u_3 &= \frac{-j}{\mu}\, g t_{33} + 2u_3^I. \end{aligned} \tag{4}$$

2.3. Wave-fields at the spacer's ends

A spacer of width w and height h (Fig. 1) has its side surfaces stress-free. Its end surfaces at $z = \pm h/2$, contacting either with the substrate or acoustic buffer, are loaded by stress $T_{u,b} = T_{33}(x)\,|_{z=\pm h/2}$; the resulting displacements are $U_{u,b} = U_3(x)\,|_{z=\pm h/2}$ (capital letters are used for wave-fields in teeth, while small letters for wave-fields concern the substrate or acoustic buffer;

note that at sliding contact, $T_{31} = 0$ and U_1 is arbitrary). These surface wave-fields are expanded in natural Fourier series over the domain $(-w/2, w/2)$ like:

$$F(x) = \sum_n F^{(n)} \exp(-jnWx), \qquad W = 2\pi/w. \tag{5}$$

In applications, the Fourier series is truncated at $|n| = N$, with N chosen sufficiently large to obtain numerically stable final results, weakly dependent on variation of N. The above can be rewritten in the matrix form: $F(x) = \mathbf{F}^T \mathrm{diag}\{\exp(-jnWx)\}$ (we use boldface letters for matrices, superscript T means matrix transposition).

The dependence of $\mathbf{U}$ on $\mathbf{T}$ results from the intrinsic dynamics of the strip. Here, we use modal expansion of the wave-field in infinite plate to evaluate both at the plate normal cross-sections z. Assuming the amplitude of the mth mode a_m, its wave-number q_m and the modal shape $F(x)\exp(-jq_m z)$, the Fourier expansion of the planar wave-field of interest are (consider $\mathrm{diag}\{\cdot\}$ as a square matrix where values of n were specified earlier in Eq. (5)):

$$\begin{aligned} U_{u,b}(x) &= \sum_m \mathbf{U}^T_{u,b} \mathrm{diag}\{\exp(-jnWx)\}\, e^{-jq_m(\pm h/2)} a_m, \\ T_{u,b}(x) &= \sum_m \mathbf{T}^T_{u,b} \mathrm{diag}\{\exp(-jnWx)\}\, e^{-jq_m(\pm h/2)} a_m. \end{aligned} \tag{6}$$

Elimination of a_m from these two equations yields explicit dependence of $\mathbf{U}_{u,b}$ on $\mathbf{T}_{u,b}$ in the matrix pseudo-impedance form (Danicki, 2010), $\mathbf{U} = \mathbf{HT}$:

$$\begin{bmatrix} \mathbf{U}_u \\ \mathbf{U}_b \end{bmatrix} = -\frac{j}{\mu} \begin{bmatrix} \mathbf{D} & \mathbf{d} \\ -\mathbf{d} & -\mathbf{D} \end{bmatrix} \begin{bmatrix} \mathbf{T}_u \\ \mathbf{T}_b \end{bmatrix}. \tag{7}$$

The column vectors $\mathbf{U}_{u,b}$ and $\mathbf{T}_{u,b}$ include $2N+1$ of the lowest Fourier coefficients each, with wave-numbers $nW, |n| \le N$; matrices $\mathbf{D}$ and $\mathbf{d}$ are evaluated numerically (Danicki, 2008).

3. The scattering problem

The surface wave fields in the periodic system of spacers, at their contact planes with acoustic buffer or the substrate is searched in the form of truncated Bloch expansion:

$$f(x) = \sum_k f^{(k)} e^{-j(r+kK)x} = \mathbf{f}^T \mathrm{diag}\{e^{-j(r+kK)x}\}, \tag{8}$$

where Λ is the period of spacers, $K = 2\pi/\Lambda$, and $r \in (-K/2, K/2)$ is the reduced wave-number belonging to the first Brillouin zone; it is the spectral variable evaluated in the boundary-value problem as the reduced wave-number of interface wave r_o, or is given by the incident wave-form $\exp(-jrx)$; hence for $p = r+kK$, the vector $\mathbf{u}^I(p)$ is $u^I(r)[\delta_{0k}]$; δ_{lk} is the Kronecker delta.

In what follows, $\mathbf{f}$ is the column vector of Bloch components of either the surface displacements u_3 or surface traction t_{33}, in the acoustic buffer $(\mathbf{u}_u, \mathbf{t}_u)$ or the substrate $(\mathbf{u}_b, \mathbf{t}_b)$. In this notation, the Eqs. (1) and (4) are:

$$\mathbf{u}_u = \mathbf{g}\mathbf{t}_u + 2\mathbf{u}^I, \qquad \mathbf{u}_b = -\mathbf{g}\mathbf{t}_b, \tag{9}$$

where $\mathbf{g} = \mathrm{diag}\{g(r + kK)\}$ and $\mathbf{u}^I$ is the corresponding column vector $u^I(r)[\delta_{0k}]$; the domain of k is that chosen in Eq. (8).

In the problems considered, the particle displacements continuity is required at the contact domains of spacers, $x \in (-w/2, w/2) + l\Lambda$ (l - arbitrary integer). Also the surface traction on the spacers ends must be equal that occurring at the spacers contact with substrate and buffer. Note however that the traction between spacers vanish. Hence, the boundary conditions

are:

$$u_{u,b}(x) = U_{u,b}(x),\ x \in (-w/2, w/2) + l\Lambda,$$
$$T_{u,b}(x) = t_{u,b}(x),\ x \in (-w/2, w/2) + l\Lambda,$$
$$t_{u,b}(x) = 0,\ x \notin (-w/2, w/2) + l\Lambda,$$

where $t_{u,b} = t_3 \mid_{z=\pm h/2}$. Applying Eqs. (6,8), they can be presented in the form:

$$\begin{aligned} \mathbf{U}_{u,b}^T \mathrm{diag}\{e^{-jnWx}\} &= \mathbf{u}_{u,b}^T \mathrm{diag}\{e^{-j(r+kK)x}\} \\ \mathbf{t}_{u,b}^T \mathrm{diag}\{e^{-j(r+kK)x}\} &= \mathbf{T}_{u,b}^T \mathrm{diag}\{e^{-jnWx}\}, \end{aligned} \tag{10}$$

for $x \in (-w/2, w/2) + l\Lambda$ (and $\mathbf{t}_{u,b} = \mathbf{T}_{u,b} = 0$ outside this domain).

These equations can be solved with respect to $\mathbf{u}_{u,b}$ and $\mathbf{T}_{u,b}$ by applying simple Fourier integrals over $x \in (-w/2, w/2)$, what yields (Danicki, 2010):

$$\begin{aligned} \mathbf{U}_{u,b} = \mathbf{V}\mathbf{u}_{u,b},\ \mathbf{t}_{u,b} = \beta \mathbf{V}^T \mathbf{T}_{u,b}, \\ V_{kn} = \frac{\sin\{(r+kK)w/2 - n\pi\}}{(r+kK)w/2 - n\pi}, \end{aligned} \tag{11}$$

where $\beta = K/W$ and $\mathbf{V} = [V_{kn}]$, the matrix which transforms the wave-fields from natural Fourier representations on strips to the Bloch representations on the substrate and buffer. It has the following property (Danicki, 2008) ($\mathbf{I}$ is a unitary matrix of corresponding dimension):

$$\beta \mathbf{V}^T \mathbf{V} \approx \mathbf{I}. \tag{12}$$

Now, after simple transformations of Eqs. (9) and (11) accounting for Eq. (7), the scattering problem is formulated by ($0\mathbf{u}^I$ is the corresponding vector of zeros):

$$\begin{aligned} (\beta \mathbf{V}\mathbf{D}\mathbf{V}^T - \mathbf{g})\mathbf{t}_u + \beta \mathbf{V}\mathbf{d}\mathbf{V}^T \mathbf{t}_b = 2\mathbf{u}^I, \\ \beta \mathbf{V}\mathbf{d}\mathbf{V}^T \mathbf{t}_u + (\beta \mathbf{V}\mathbf{D}\mathbf{V}^T - \mathbf{g})\mathbf{t}_b = 0\mathbf{u}^I. \end{aligned} \tag{13}$$

There are two separated systems of equations for symmetric and antisymmetric wave-fields in the considered symmetric system, where the substrate and acoustic buffer are made of the same material. Solving these equations, one easily obtains normal traction on the substrate $\mathbf{t_b}$ and normal displacement from Eq. (1), particularly its Bloch components with wave-number $r + kK \approx \pm k_R$ determining the acoustic power transportation along the substrate, Eq. (3).

4. Interface wave-modes

It is evident that perhaps two interface modes can exist; their reduced wave-numbers r_o can be evaluated from Eqs. (13) which, after applying Eq. (12), yield:

$$\det(\mathbf{D} \pm \mathbf{d} - \beta \mathbf{V}^T \mathbf{g} \mathbf{V}) = 0. \tag{14}$$

In the applied teeth geometry ($w = \lambda_R/4$ and $h \leq w$), only one mode exists with $r_o^2(K)$ well approximated by:

$$r_o^2 = (K - K_1)(K - K_2 + j\chi), \tag{15}$$

where $K_{1,2}$ are the stopband edges where $\mathrm{Re}\{r_o^2\} = 0$, the stopband width is $K_2 - K_1$, and χ, representing the SAW damping due to the radiation of bulk waves into the substrate, describes the linear dependence of $\mathrm{Im}\{r_o^2\}(K)$ for the considered domain of K in vicinity of the stopband. In all the presented examples, wave-numbers are scaled down by 2π, the applied $k_t = 2\pi$ is presented as 1, and $k_l = 0.4723 k_t$ as 0.4723, similarly for K and r_o^2, *etc.*; and h is scaled down by w ($h = w$ is presented as 1) where w is a quarter of the Rayleigh wavelength.

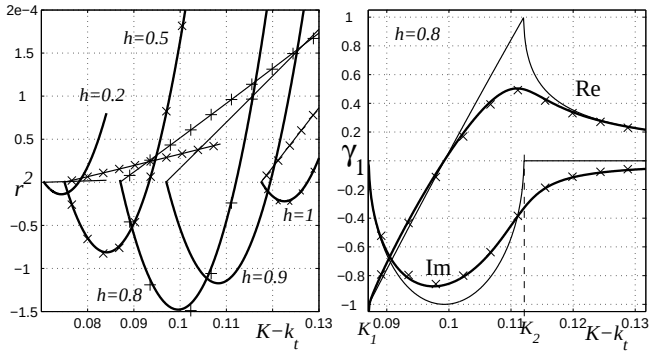

Figure 2: Characterization of the interface mode. Solid lines represent numerical results evaluated directly from Eqs. (13), (14), and crosses show approximations evaluated from Eq. (15) and (17). Left: pseudo-dispersive curves $r_o^2(K)$ presenting stopbands where $\mathrm{Re}\{r_o^2\} < 0$. Presented for different h, the nearly parabolic curves of $\mathrm{Re}\{r_o^2\}$ and the corresponding linear $\mathrm{Im}\{r_o^2\}$ move to the right for growing h. Wave-numbers r_o are scaled down by 2π (note that r_o^2 is of an order 10^{-4}) and h is presented respective to w. Right: the modal shape γ_1; thin lines show the 'ideal' γ_1 when $\chi = 0$, with $|\gamma_1| = 1$ in stopband.

The modal shape in the substrate is determined by the corresponding null vector $[\mathbf{t}_u; \mathbf{t}_b]$ of the matrix of Eqs. (13), the most important components of which (Bloch orders) involved in acoustic power transfer, ref. Eq. (3), are $t_b^{(\pm 1,0)}$ and

$$\begin{aligned} u_b^{(\pm 1)} &= \frac{j}{\mu} g(r_o \pm K) t_b^{(\pm 1)}, \\ u_b^{(0)} &= \frac{j}{\mu} g(r_o) t_b^{(0)}. \end{aligned} \tag{16}$$

For $r_o \approx 0$, the corresponding SAWs of amplitudes $a_{\pm 1} \sim u_b^{(\pm 1)}$ evaluated from Eq. (3) at wave-numbers $r_o \pm K \approx \pm k_R$, carry acoustic power to the right and to the left on the substrate surface, while $u_b^{(0)}$, having small wave-number below the cut-off wave-numbers of bulk waves, indicate power leakage, what causes interface wave damping and r_o to be complex-valued.

For r_o with imaginary part $r_I = \mathrm{Im}\{r_o\} > 0$, as presented in the computed examples, the wave-field vanishes on the substrate surface at $x \to -\infty$, indicating that this is the interface wave propagating to the left. Naturally, the wave component $u_b^{(-1)}$, having wave-number $r_o - K \approx -k_R$, is responsible for the power transport to the left. The other component, $u_b^{(+1)}$, having wave-number $r_o + K \approx k_R$, carries the power to the right. The net power transported by the considered mode to the left is the difference between these two; this phenomenon was thoroughly investigated in the theory of SAW interdigital transducers (Danicki, 2007). The exact relation derived there between the forward and backward Bloch components suggests the following approximation (which verification is presented in Fig. 3):

$$\begin{aligned} \gamma_1 = \frac{u_b^{(+1)}}{u_b^{(-1)}} \approx \frac{k' - r_o}{k' + r_o}, \\ \gamma_0 = \frac{u_b^{(0)}}{u_b^{(-1)}}, \end{aligned} \tag{17}$$

where $k' = K - K_1$. In the considered symmetric structure, Eq. (17) holds for $u_u^{(\pm 1)}$, as well. Note that $|\gamma_1| \to 0$ for growing k' and $|\gamma_1| \approx 1$ for close to imaginary valued r_o (in stopband).

As discussed above, the 0th Bloch component, $u_b^{(0)}$, excites the bulk waves (primarily longitudinal for small r_o) that carries power P down the substrate, naturally at the cost of the interface wave power, making it decaying. Repeating the considerations based on the power balance, Eq. (3), but accounting for the fact that the interface wave power Π is the difference of powers $\Pi_{\pm 1}$ carried in opposite directions by ± 1 Bloch orders, and introducing the

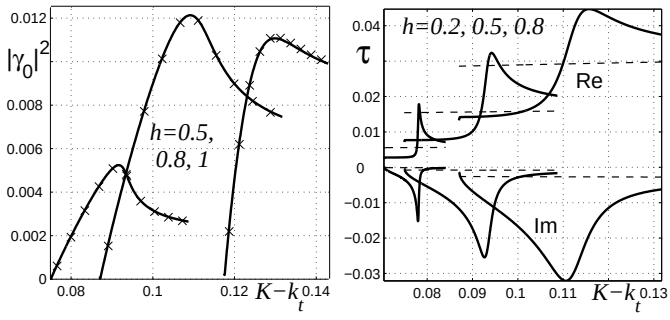

Figure 3: Left: the interface wave leakage (lines) compared with the wave damping (crosses), verifying Eq. (18). Right: excitation strength τ and verification of $\tau(1-\gamma_1) \approx$ const (dashes). In all drawings, the curves from left to right correspond to growing h (*cf.* Fig. 2), taking values of 0.5, 0.8 and 1, respective to w.

notation $r_o = r_R + jr_I$ $(r_I > 0)$, we obtain:

$$2r_I(\Pi_{-1} - \Pi_{+1}) = P,$$
$$\Pi_{\pm 1} = |\frac{\dot{g}_{\pm 1}}{2}|\mu\omega|u_b^{(\pm 1)}|^2/2, \qquad \dot{g}_{\pm 1} = |\dot{g}(r_R \pm K)|,$$
$$P = Z_l(k_l^2 - r_R^2)^{-1/2}|\omega u_b^{(0)}|^2/2$$

(accounting for slightly off-normal outgoing bulk waves excited by the discussed leakage phenomenon and represented by wave-vector x-component $r_R \neq 0$; although any r_R can be achieved in a periodic systems, the comb period Λ is chosen approximately equal the Rayleigh wavelength in order to obtain small value of r_R). Finally:

$$|\gamma_0|^2 = \frac{r_I\sqrt{k_l^2 - r_R^2}}{k_t^2}(\dot{g}_{-1} - \dot{g}_{+1}|\gamma_1|^2), \tag{18}$$

which equation is nicely satisfied in our computations presented in Fig. 3. This verifies our understanding of the discussed leaky interface waves and shows the computation accuracy; numerical details are presented in (Danicki, 2010).

5. Excitation of interface waves

Having satisfactory approximations for free-propagating interface wave amplitudes and powers, we seek only the amplitude of the generated interface wave (sufficiently characterized by $u_b^{(0)}$, for instance) by scattering of incident bulk waves on spacers. This is governed by Eq. (13), from which it follows that:

$$\mathbf{u}_b(r) = \mathbf{M}\backslash[\delta_{0k}]u^I(r) \Rightarrow u_b^{(0)}(r) = u^I(r)f(r), \tag{19}$$

where f, corresponding to the inverse matrix $\mathbf{M}^{-1}$, is singular at r_o, that is $f^{-1}(r_o) = 0$.

In typical cases, the normal incident wave-beam aperture width A is large and its spatial spectrum $u^I(r) = 2\sin(rA/2)/r$ is well confined in $(-K/2, K/2)$ (its higher Bloch orders involved in Eq. (19) are negligible). Naturally, only this part of the spectrum excites the interface wave which is closer to the wave-number $r_R \approx 0$. Other part of the wave-beam spectrum excites only the localized vibration around teeth. We neglect the localized part of the generated wave-field, seeking only the propagating part of the spatial solution to $u_b^{(0)}(x)$ which is the inverse Fourier transform of $u_b^{(0)}(r)$:

$$u_b^{(0)}(x) = \frac{1}{2\pi}\int_{-K/2}^{K/2} u_b^{(0)}(r)e^{-jrx}dr \approx \frac{1}{2\pi}\int_{-\infty}^{\infty} u_b^{(0)}(r)\, e^{-jrx}dr, \tag{20}$$

where we extend the integration limits to infinity (the added integration path can only contribute to the localized wave-field, being of least interest to us), the interesting solution at $x < -A/2$ (just outside the incident wave-beam)

is (note that for $\mathrm{Im}\{r_o\} > 0$, the integral (20) converges if $x < -A/2$):

$$u_b^{(-1)}(x) = u_b^{(0)}/\gamma_0 = j\tau u^I(r_o)e^{-j(r_o-K)x},$$
$$\tau = [d\, f^{-1}(r)/dr]_{r_o}^{-1} = k_t b/(1-\gamma_1), \qquad b \approx \text{const}, \tag{21}$$
$$u_b^{(+1)} = \gamma_1 u_b^{(-1)}, \qquad a_{\pm 1}^G = u_b^{(\pm 1)}\sqrt{\mu\omega|\dot{g}_{\pm 1}/2|}.$$

The parameter τ characterizes the generation of interface wave in the system. Analogous results can be obtained for $x > A/2$, that is for the interface wave propagating to the right, one only has to replace r_o by $-r_o$ and $u_b^{(\pm 1)}$ by $u_b^{(\mp 1)}$. The numerically evaluated excitation strengths of interface waves τ are presented in Fig. 3 for several spacers' height h (again presented relative to $w = \lambda_R/4 \approx \Lambda/4$). The results confirm that $b = \tau(1-\gamma_1)/k_t \approx \text{const}$ what will be exploited in the next section.

6. Comb transducer efficiency

The above results concern generation of interface waves by the plane incident wave. Now, they are exploited for modeling comb of finite width, what is equivalent to the incident wave-beam of the finite aperture width, characterized at the interface plane by its spatial spectrum. Later below, we will analyze finite comb working as surface wave receiver by means of conversion of SAWs into interface waves which by the leaky mechanism excite bulk waves in the comb buffer at the comb-substrate finite contact area. These bulk waves are eventually detected at the other end of the buffer by piezoelectric transducer. In both cases we meet very difficult scattering problem at the comb edges. Here, we apply useful approximation verified in theory of shallow groove-grating reflectors (Field et al, 1975), which we believe is also sufficient for estimation of comb transducer efficiency.

6.1. Generation of surface waves

An incident bulk wave of aperture width A (propagating in the comb buffer of the same dimension), symmetric with respect to central spacer (Fig. 1), excites the interface wave-fields at the left comb end on the strength of Eq.(19) and later:

$$a^G_{-1} = a_G \exp(-j(r_o - K)x), \text{ and}$$
$$a^G_{+1} = \gamma a_G \exp(-j(r_o + K)x) \text{ at } x = -A/2,$$

where $\gamma = \gamma_1[\dot{g}(r_o+K)/\dot{g}(r_o-K)]^{1/2}$. These Bloch components carry acoustic power along the substrate surface correspondingly to the left and to the right. Similarly at the right comb end $x = A/2$ the excited wave-fields are:

$$a^G_{+1} = a_G \exp(j(r_o - K)x), \text{ and}$$
$$a^G_{-1} = \gamma a_G \exp(j(r_o + K)x),$$

analogously carrying power correspondingly to the right and to the left. In both cases, the power transfer by the wave components with amplitude a_G prevails, so that $a_G \exp(j(r_o - K)A/2))$ transfers larger acoustic power out of the comb area than the power of $\gamma a_G \exp(j(r_o + K)A/2)$ that is reflected back into the comb domain (*cf.* schematic diagram in Fig. 1).

Additionally, inside the comb area ($-A/2 < x < A/2$), free propagating interface waves may exist (propagating either to the left with wave-number r_o, or to the right with wave-number $-r_o$ as presented by the diagram in Fig. 1), both composed of the forward and backward Bloch components: $a^{\mp} \exp(\pm j(r_o-K)x), \gamma a^{\mp} \exp(\pm j(r_o+K)x)$.

In the area outside the comb, free propagating Rayleigh waves may exist: the propagating to the left or to the right on the left or right-hand side of

the comb,

$$\tilde{a}_L^{\mp} = a_L^{\mp} \exp(\pm j k_R x), x < -A/2, \text{ and}$$
$$\tilde{a}_R^{\pm} = a_R^{\pm} \exp(\mp j k_R x), x > A/2,$$

respectively. We assume here that there is no power loss at the comb edges (as may be caused by scattering into bulk waves, for instance) and that all wave-mode shapes are similar (that is $\dot{g}$ evaluated at $r_R \pm K, k_R$ are close to each other). This enables us to apply the following conservative boundary conditions (Field et al., 1975) at $x = -A/2$ (again, ref. Fig. 1):

$$\begin{aligned} a_G e^{j(r_o-K)A/2} + a^- e^{j(r_o-K)A/2} + \gamma a^+ e^{j(r_o+K)A/2} &= \tilde{a}_L^-, \\ \gamma a_G e^{j(r_o+K)A/2} + \gamma a^- e^{j(r_o+K)A/2} + a^+ e^{j(r_o-K)A/2} &= \tilde{a}_L^+; \end{aligned} \tag{22}$$

the equations at $x = A/2$ are similar; one needs only to replace superscripts $+, -$ by $-, +$ and subscripts L, R by R, L.

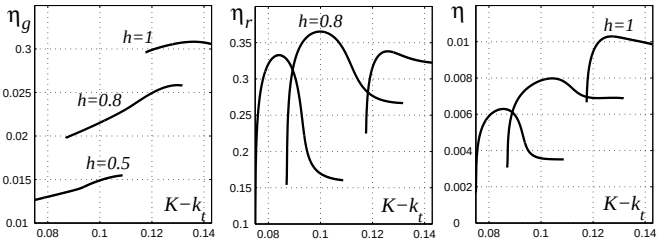

Figure 4: Estimated properties of combs with 11 teeth and different teeth heights: $0.5w, 0.8w$ and $1w$ (for curves from left to right in all figures). Left: generation efficiency. Middle: comb receiver efficiency. Right: approximated combined efficiency $\eta = \eta_g \eta_r$ of a pair of generating and receiving combs.

Evaluation (from Eq. (19) and earlier) of the free interface waves $a^{\pm}$ bouncing between the comb edges yields the generated Rayleigh wave ampli-

tude at the left-hand side of the comb:

$$\tilde{a}_L^- = jbu^I(r_o)k_t\sqrt{\mu\omega\dot{g}_{-1}/2}\;\frac{e^{j(r_o-K)A/2}}{1-\gamma_1}\frac{1-\gamma^2}{1+\gamma e^{jr_oA}},$$
$$\gamma = \gamma_1\sqrt{\dot{g}_{+1}/\dot{g}_{-1}}, \tag{23}$$

where $u^I(r_o) = 2u^I\sin(r_oA/2)/r_o$ for uniform normal incident wave-beam of aperture width A and displacement amplitude u^I, carrying the incident power $P^I = AZ_l|\omega u^I|^2/2$, where $Z_l = \rho\omega/k_l$ is acoustic impedance of the comb buffer. For small r_o, particularly at the stopband where $r_R \approx 0$, $\gamma \approx \gamma_1$, the comb transducer generation efficiency is:

$$\eta_g = \sqrt{\frac{|a_R|^2}{2P^I}} = |b|\sqrt{k_lA\frac{\dot{g}_{-1}}{2}}\,|\frac{(1-e^{jr_oA})(1+\gamma_1)}{r_oA(1+\gamma_1e^{jr_oA})}|. \tag{24}$$

Note however that there are equal generated SAW in both the substrate and the acoustic buffer, the latter assumed to be entirely scattered and damped in the buffer. This, naturally, lowers the transducer efficiency presented in (Fig. 4), yielding only about 10% of the incident wave power transformed into SAWs in the substrate. It is worth to note here that the generated SAWs in both the substrate and the buffer have the symmetry of the existing interface mode (the only one in the applied range of values of h in this paper).

6.2. Detection of surface waves

Eqs. (22) allow us to evaluate the outgoing SAWs: a_L^-, a_R^+, for example resulting from the incident SAW a_L^+:

$$a_L^- = \gamma a_L^+\frac{e^{jr_oA}-e^{-jr_oA}}{\gamma^2e^{jr_oA}-e^{-jr_oA}},$$
$$a_R^+ = a_L^+\frac{\gamma^2-1}{\gamma^2e^{jr_oA}-e^{-jr_oA}}. \tag{25}$$

Note however that they are evaluated under the assumption that there are incident SAWs in both the substrate and the acoustic buffer of the corresponding symmetry mentioned above. If there is only the incident SAW of amplitude a_L in the substrate, it must be split into symmetric and antisymmetric SAW pairs propagating in both the half-spaces. The symmetric pair meets a barrier in the comb-substrate interface because no interface wave of this symmetry exists. Hence this pair of SAWs must be entirely reflected and scattered at the comb edge. We neglect this pair entirely in the following discussion by applying an equivalent incident SAW amplitude $a_L^+ = a_L/\sqrt{2}$ in Eq. (25).

Comparing the incident SAW power $|a_L|^2/2$ with the reflected and transmitted wave powers $|a_L^-|/2 + |a_R^+|^2/2$ we notice that there is a certain imbalance resulting from the power leakage into the bulk waves in the comb area (the interpretation verified earlier in Fig. 3); in the stopband, these waves propagate almost perpendicularly to the comb-substrate interface (due to $r_R \approx 0$, as discussed earlier) to be eventually detected by a piezoelectric transducer on the other end of the acoustic buffer. Hence, this power imbalance is a signature of the receiving comb efficiency in transforming the incident SAWs into bulk waves in the acoustic buffer. The same power propagates down the substrate in the considered system where both media are of the same material; this power is lost diminishing the comb overall efficiency.

Summarizing, we obtain the approximation for the comb transducer receiving efficiency:

$$2\eta_r^2 = 1/2 - |a_L^-/a_L|^2 - |a_R^+/a_L|^2, \tag{26}$$

where we have accounted for the half-power loss introduced by the symmetric

SAWs pair discussed above and another half-power loss due to the undetected scattered bulk waves in the substrate. Fig. 4 presents $|\eta_r|$ for an example comb counting 11 teeth, for different teeth height.

In typical applications, the same comb or a pair of combs generate and receive SAWs in the system. The total efficiency of bulk wave transformation to surface waves and back to bulk waves can thus be estimated as $\eta = \eta_g \eta_r$, the examples of which shown in Fig. 4 indicate the best efficiency at stopband.

7. Conclusions

The presented analysis explains certain fundamental phenomena partaking in the bulk to surface wave transformation in comb transducers which cannot be analyzed on the basis of perturbation theory that assumes weak mechanical interaction between comb teeth and the substrate, and that the teeth vibrations generate directly the Rayleigh waves which propagate freely at the comb-substrate interface.

The presented theory has shown that leaky interface waves are generated instead, propagating to the left and to the right along the interface. Due to the teeth periodicity, both these interface waves are composed from forward and backward Bloch components carrying acoustic powers in different directions. Moreover, the 0th Bloch order component excite the bulk waves in both the comb and the substrate media, what is the reason of interface wave damping. Fig. 3 nicely verifies this physical interpretation.

The interface waves are subjected to Bragg reflection, typical for periodic systems. It is found that the resulting stopband is best visible in drawing of $r_o^2(K)$, when $\mathrm{Re}\{r_o^2\} < 0$. It is also found that $\mathrm{Im}\{r_o^2\} > 0$ is a linear

function of K, vanishing at the stopband edge K_1 (Fig. 2). This implies that the 0th Bloch order component vanishes there. The approximate relations characterizing the Bragg reflection phenomenon presented in Eqs. (15) and (17) have been found valid (with good accuracy) in the presented numerical examples.

The last figures (Fig. 4) present a general property of comb transducer having practical, moderate number of eleven teeth. It is seen that the generating comb exhibits the best efficiency just above the right stopband edge K_2. The comb working as a receiver of surface waves however, is efficient at the stopband. In typical arrangement of a pair of combs for generation and detection of SAWs, the best efficiency $\eta = \eta_g \eta_r$ is obtained again at the stopband. The presented examples show that the insertion loss in such a measurement arrangement is about 40dB (neglecting the efficiency of piezoelectric transducers), what is a quite good result.

The passband width of a pair of combs is determined by the interface wave stopband, that is rather narrow (few per cent) in the presented examples. Note however, that in this paper we present pseudo-dispersive dependence of r_o on K, not on ω. Changing the frequency ω, the relative teeth height and width will vary along with the relative teeth period with respect to the SAW wavelength. These changes, when cumulated, may yield somewhat different results concerning passband. Analyzing them all is far beyond the scope of this paper, dedicated primarily to the fundamental theory of comb transducers. Future investigation should concern primarily the comb of different material from the substrate. Plastic, instead of metal spacers may be interesting as better adhering to a rough substrate surface.

References

Danicki, E. J., 1999. Resonant phenomena in bulk-wave scattering by in-plane periodic cracks, J. Acoust. Soc. Am. 105, 84–92.

Danicki, E. J., 2007. Spectral theory of interdigital transducers of surface acoustic waves, *http://www.ippt.gov.pl/∼edanicki/danickibook.pdf*, Chapt. 1 and 4.

Danicki, E. J., 2008. Evaluation of planar harmonic impedance for periodic elastic strips of rectangular cross section by plate mode expansion, ASME J. Appl. Mech. 75, 041011-1–6.

Danicki, E. J., 2010. Interface wave-modes in comb transducers, Wave Motion 47, 508–518.

The general derivation presented there includes both the displacement U_i and traction $T_i = T_{3i}$, $i = 1, 3$, from which, applying $T_1 = 0$, Eq. (7) results:

$$\begin{bmatrix} \mathbf{U}_1^u \\ \mathbf{U}_3^u \\ \mathbf{U}_1^b \\ \mathbf{U}_3^b \end{bmatrix} = \frac{-j}{\mu} \begin{bmatrix} \mathbf{A} & \mathbf{B} & \mathbf{a} & \mathbf{b} \\ \mathbf{C} & \mathbf{D} & \mathbf{c} & \mathbf{d} \\ -\mathbf{a} & \mathbf{b} & -\mathbf{A} & \mathbf{B} \\ \mathbf{c} & -\mathbf{d} & \mathbf{C} & -\mathbf{D} \end{bmatrix} \begin{bmatrix} \mathbf{T}_1^u \\ \mathbf{T}_3^u \\ \mathbf{T}_1^b \\ \mathbf{T}_3^b \end{bmatrix}$$

.

Field, M. E., Ho, R. C., Chen, C. L., 1975. Surface acoustic wave grating reflector, in IEEE Ultras. Symp. Proc., 430-433.

Hurley, D. C., 1999. Nonlinear propagation of narrow-band Rayleigh waves excited by a comb transducer, J. Acoust. Soc. Am. 106, 1782-1788.

Ingebrigtsen, K. A., 1969. Surface waves in piezoelectrics, J. Appl. Phys. 40, 2681–2686.

Victorov, I. A., 1967. Rayleigh and Lamb waves: Physical theory and applications, Plenum Press, New York.